Graphene-based rectennas for energy harvesting

Position paper of the Horizon 2020 project GreEnergy

By Per Lundgren, Muhammad Hassan, Per Rudquist (Chalmers University of Technology), Andreas Hemmetter, Avi Ginzburg, Zhenxing Wang, Max C. Lemme (AMO GmbH), Kirsten Leufgen, Clara Roujeau, Wolf-Peter Ulrich (SCIPROM Sàrl), Mesut Inac, Mindaugas Lukosius (Leibniz Institut für innovative Mikroelektronik), Yuval Baryossef (Nogah Photonics Ltd), Emiliano Laudadio, Davide Mencarelli, Luca Pierantoni (Università Politecnica delle Marche), Fooqia Khalid, Naveed Mehmood, Harri Lipsanen (Aalto University), Davide Truccolo, Stefano Boscolo, Michele Midrio (University of Udine)

In the 4-year EU Research Project GreEnergy, we have focussed on the concept of energy harvesting from solar antennas, from individual components to system level, with the aim of achieving a proof of concept. For each single component we have aimed to advance the state of the art, theoretically as well as experimentally, and to identify the bottlenecks for future exploration.

In this position paper we summarize our achievements and discuss some important aspects and challenges for future advances and realization of energy harvesting from solar antennas. The enhancement of the rectification and the impedance matching between nano-antennas and the rectifier stand out as major tasks in the pursuit of research in this field.

GreEnergy
Power from optical antennas

Introduction

Global warming is a major threat to our planet and is mostly caused by the extensive burning of fossil fuels. The annual global energy consumption (620 EJ) and energy-related greenhouse gas emissions (40 Gt CO_2e) have both reached a new record in 2023. Rapid decarbonization of the energy production is therefore crucial.[1] It is also well-known that solar energy is the most powerful energy source of our planet and, moreover, it is freely available. Solar energy hits earth with a power of 1.08×10^{14} kW. If we were able to capture only 0.1% of this energy and convert it to useful energy at an efficiency of 10%, we would during each second generate four times the world's annual total energy needs.[2] In addition, harvesting solar radiation on a miniature scale opens the way to various autonomous solar-powered microelectronic devices and systems, as well as extending the applications for which such energy harvesting is applicable.

During recent decades we have seen a tremendous increase of solar cell-based electricity generation, both on a large industrial scale, and on a smaller scale (e.g. in private homes and buildings). Solar cells transform sun light directly into electricity through the photoelectric effect. Such photovoltaic (PV) silicon-based solar cells are mature and reliable, although the efficiency is limited to about 20% for a single layer device. The theoretical maximum efficiency limit for photovoltaics is about 33% (for single junction cells) and with highly sophisticated and expensive heterogeneous structures, efficiencies up to almost 50% have been reported in laboratories.[2]

Recent advances in nanotechnology, and in particular, in nano-fabrication, have revived the interest in another type of solar energy harvesting mechanism, proposed already more than 50 years ago[3], based on optical antennas coupled to ultra-high-speed diodes. Here electromagnetic waves picked up by the antenna results in an alternating current with the same frequency as the incoming light, which is subsequently rectified into direct current by the diode (rectifier). In theory, such an optical rectenna (rectifier plus antenna) could provide a much higher harvesting efficiency than photovoltaics, limited only by thermodynamic considerations, and could be larger than 80%. Rectennas have been manufactured and demonstrated at microwave frequencies, but not for optical nor near IR frequencies, which would be needed for solar energy harvesting.

The main challenges for realization of optical frequency rectennas are:

1. As the dimensions of a receiving antenna must be fractions of the wavelength of the waves being received, antennae for optical frequencies must be of the order of tens of nanometres. Even with the most modern nanofabrication tools and processes, such nanometric metallic structures are extremely difficult to produce reliably.

2. The frequency of visible light is about 10^{14} Hz, and even the fastest electronic diode has not been proven yet to operate at frequencies of visible nor even near IR light.

Because of 1 and 2, rectification of sunlight has been considered a very ambitious challenge ever since Baileys suggested it in 1972. However, after several decades of development of nanofabrication technology, which has pushed back the limits of manufacturing resolution to ever smaller dimensions, in combination with the advent of high-performing materials such as graphene, it is now relevant to make a serious attempt to take the next steps towards the ultimate goal of optical rectennas for solar energy harvesting.

List of abbreviations

CA
Consortium Agreement

DoA
Description of Action

FOM
Figure of merit

GA
Grant Agreement

PCL
Photon Coherence Length

WRA
Wideband Rectenna Array

Funded by the EU's Horizon 2020 programme, the GreEnergy project [4], a consortium consisting of Chalmers University of Technology (Sweden), AMO GmbH (Germany), SCIPROM Sàrl (Switzerland), IHP GmbH (Germany), Nogah Photonics (Israel), Ancona University UNIVPM (Italy), Aalto University AALTO (Finland) and University of Udine UNIUD (Italy), has addressed the concept of rectenna-based solar energy harvesting, from individual components to system level, to conduct a proof of concept. The aim is to identify and exceed the state of the art in all the necessary components and sub-systems. Importantly, a main ambition of GreEnergy has been to explore technologies which we consider to be scalable for future volume production. We have, for example, focussed on CVD graphene rather than possibly better-performing exfoliated and/or hexa-boron nitride (hBN)-encapsulated graphene, as the use of exfoliated graphene layers for electronics devices requires hands-on manipulation of individual atomically thin flakes, which is not scalable. The conducted research includes the top-down system processes (AMO), system modelling and circuitry (Chalmers, IHP), rectenna modelling and design (UNIVPM, UNIUD), rectenna prototype manufacturing and characterization, (AMO, AALTO), supercapacitor design, manufacturing and characterization, (Chalmers), and integration of rectennas and supercapacitors on a single chip (Chalmers).

Partner short names

Chalmers – Chalmers Tekniska Hoegskola AB

AMO – Gesellschaft für Angewandte Mikro-und Optoelektronik mbH

SCIPROM – SCIPROM Sàrl

IHP – IHP GmbH - Innovations for High Performance Microelectronics / Leibniz-Institut fuer Innovative Mikroelektronik

NOGAH – NOGAH PHOTONICS LTD

UNIVPM – Università Politecnica delle Marche

Aalto – Aalto Korkeakoulusaatio SR

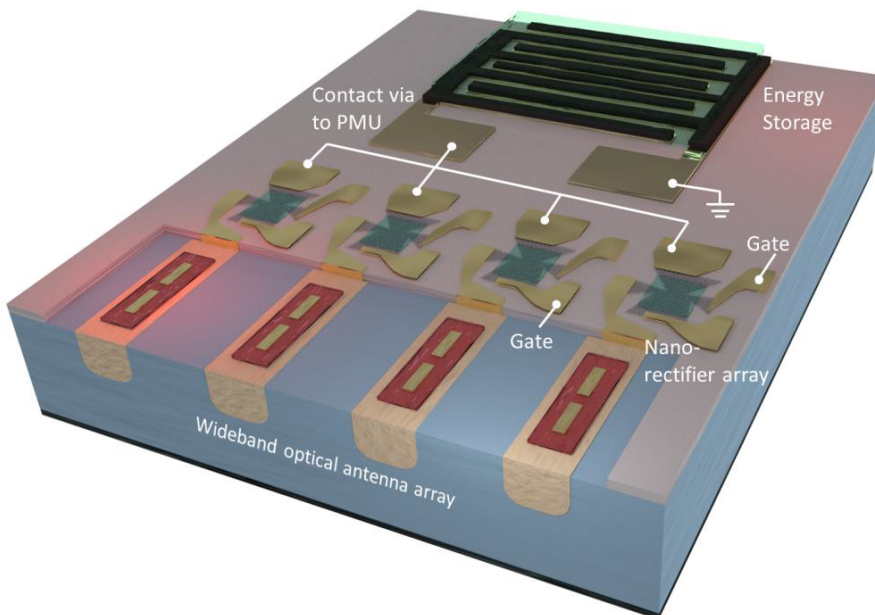**UNIUD –** Università degli Studi di Udine

Figure 1. Schematic picture of envisaged combined harvesting and storage device. In the work we have chosen to integrate the antenna and the rectifier in the same component, i.e. the rectenna.

In this GreEnergy position paper we describe and discuss a fully integrated, hypothetical harvesting-storage system, from the nano-antenna capturing the solar electromagnetic waves, via the rectifying diode, and the matching electronics, to micro-supercapacitor storage units, all integrated on the same chip, as schematically illustrated in Figure 1. In each of the individual parts, we have sought to identify any bottlenecks that need to be addressed in future work, at the system, component and even material level. We have shown by means of various strategies of computer simulations how absorption of sunlight using cleverly designed nanoantenna arrays indeed can be pushed beyond current state-of-the-art, and that ballistic geometric diodes of graphene might be a candidate for the rectification. Earlier work on high frequency diodes have to a large extent been focussed on metal-insulator-metal (MIM)-devices. However, to our experience the intrinsic high capacitance of MIM devices is incompatible with the low impedance of the nanoantennas which inevitably results in huge insertion losses. As we will discuss, even with the lower impedance ballistic graphene-diodes, the impedance matching and frequency response is a critical issue.

We first briefly describe the main achievements of the GreEnergy project. Then, we go into detail about some of the main results and considerations related to each part of the combined harvesting and storage system. We are focussing on the design, simulation and manufacture of the rectennas, as we consider these issues to be particularly important and critical at this stage in the development of solar rectennas.

GreEnergy accomplishments

Simulations

Although the basic ideas of nano antennas and ballistic rectifiers are well-known, they are based on simple, idealized situations. In real systems, the situation is immensely more complex, and all physical mechanisms involved, down to quantum level, are likely not yet fully understood, nor even identified. A rigorous analysis of all relevant phenomena involves simulations on a vast range of length scales, from atomic distances up to millimetres, i.e., over seven orders of magnitude(!). We have therefore developed a unique "multi-physics toolkit" that allows for simulation and development of nanoantennas, graphene diodes, as well as of complete rectennas. On a higher level, we have developed a general simulation software for the design of complete harvesting-storage system layouts, based on the individual characteristics of each component.

Components, design, manufacturing and integration

We have designed and fabricated novel high-performing antenna structures for down to visible wavelengths. However, despite elaborate efforts, we are yet to realize the nanometre-sized rectenna structures needed for these wavelengths. During the latter part of the project we therefore decided to focus on larger rectennas for longer wavelengths (frequencies in the terahertz (THz) range) for a proof of principle for the functioning of complete rectennas. We have shown that such rectennas can be manufactured and that they can transform THz radiation into DC, even if the efficiency still is very small. Importantly, we have also demonstrated that these rectennas can be integrated with micro-supercapacitors, on the same chip, well within the limitations in thermal budgets related to graphene processing.

System

For a complete energy harvesting system it is not only the efficiency of a single rectenna component that counts. We must also early on in the process address the "macroscopic problem", e.g. how much power can in the end be produced per surface area. There is currently a very significant amount of work remaining before it can be shown to what level of efficiency a graphene-based nanoscale structure can exploit ballistic transport phenomena to produce conversion between the broadband radiative power captured by the antenna array and a DC output. What can be appreciated by a system level simulation with integrated rectennas and energy storage elements (e.g., in the form of electrochemical capacitors), is, to a large extent, the trade-off consideration between low resistive losses in interconnects and use of chip surface real estate – the exposed surface should be used for power conversion, not for mere transport of DC power.

In principle, our results in GreEnergy pave the way for future complete harvesting and storage devices, although losses are still too high to allow efficient charging

of integrated supercapacitors using irradiation from rectangular antennas. The main challenges of solar rectennas for energy harvesting are still, despite decades of development of nanofabrication, related to the fabrication of the extremely small structures needed to match the wavelengths of visible light. We are convinced that multi-scale simulations and modelling of structures, components and materials are essential for future work, especially to identify the nanostructures and geometries that possibly combine high performance (efficiency) with manufacturability.

System engineering approach

Within the GreEnergy project we have used a system engineering approach and methodology to develop the harvesting module schematically depicted in Figure 1. The first stage comprised extensive simulations and design of the system and of all the individual components. After several design reviews and drafting of specifications we started with prototype manufacturing and measurements. In particular, the highly absorptive antenna structure developed through computer simulations was later used in the rectenna fabrication, and the focus on the four terminal ballistic diode is based on the results from simulations. The simulations also highlighted the importance of impedance matching, and in principle some strategies on how this problem can be attacked in the future. In parallel, we modelled the overall harvester - storage system with focus on the use of device area, and on the circuitry between the subcomponents of the GreEnergy system.

System modelling

There are several assumptions and boundary conditions that need to be established to model and evaluate system performance, to get an estimate for the overall power conversion efficiency. One such aspect concerns the fluctuations in irradiance that the system is expected to operate under. We have chosen not to go into detail on these issues in this position paper. Another fundamental boundary condition relates to the lateral Photon Coherence Length (PCL). In short, the PCL will determine the lateral maximum size of the array of antenna elements that can be integrated for constructive rectification. If each array is larger than the PCL, either the antenna area is simply wasted or, worse, there would be risk of destructive interference in the array from incoherent radiation. On the other hand, if the array is much smaller than the PCL, we would make it unnecessarily difficult to combine or integrate the different arrays on the chip, with increased losses and reduced efficiency as a consequence. The PCL has been reported to be on the order of 50 μm.[5] The dimensions of the designed and simulated rectenna arrays are smaller than this value (see "Rectenna modelling and impedance matching").

From a system simulation perspective, the Wideband Rectenna Array (WRA) is a "black box" that converts radiation to DC-power at a certain efficiency, and we therefore use an idealized DC-power source model to describe the output from the WRA. This of course makes the simulations overly optimistic in terms of performance, but they should still result in valid conclusions regarding design choices for the WRA, e.g., when considering the aim to providing high current (sources in parallel) or high voltage (sources in series).

The interconnects between WRAs are represented as resistors with a resistance that depends on material properties (represented by a bulk resistivity value) and

geometry (which includes geometry induced increases in effective resistivity.[6,7] In the simplest model, we can use an empirical description of the resistivity of the following format, which will probably underestimate the effects of geometry:

$$R = \frac{\rho \cdot 2 \cdot PCL}{LW^2}$$

$$\rho = \rho_0 \cdot \left(1 + \frac{50}{LW}\right)$$

Here R is the interconnect resistance required to bring a DC signal from a single WRA with a length equal to the PCL in connection with its surroundings, ρ is the resistivity and ρ_0 is its bulk value. A quadratic interconnect cross-section is assumed. The empirical description of the resistivity's dependence on Line Width (LW) captures increased surface scattering at small dimensions (with LW given in nanometres). The factor of 2 in Equation 1 takes into consideration that the WRA will need to have a connection to both terminals. We further presume that some low-loss via-solution can be implemented to in principle connect each WRA to an energy storage element underneath.

With the assumption that each WRA will act as an ideal DC current source, (the way a traditional photovoltaic power converter would be modelled for high impedance loads) we can obtain the power lost in each connection, P_{IL} as:

$$P_{IL} = I^2 \cdot R = \left(\frac{P_{WRA}}{U}\right)^2 \cdot R$$

The resistance R is given by the design choices for the interconnects and the geometry of the WRA. The voltage level U is here a design choice for the WRA, given also constraints or demands from the storage unit – and/or from the interfacial circuitry. If the size of the WRA is directly set by the PCL this simple analysis shows that large WRAs will perform very poorly with thin LW, whereas small WRAs will suffer severe loss of active area with wide connecting lines. For example, with, and PCL=50 um the total effective losses due to interconnections (geometric plus resistive) will be minimized at a LW close to 100 nm, and be ~15 % percentile units worse for a linewidth LW of 10 nm (resistive losses dominating), and ~8 percentile units worse for LW=1000 nm (loss of effective area dominating). Evidently, on a macroscopic level, there is a trade-off consideration between low resistive losses in interconnects and use of chip surface real estate – the exposed surface should be used for power conversion, not for mere transport of DC power.

Rectenna modelling and impedance matching

In any harvesting system that comprises rectennas, the final efficiency consists of two parts:[8] 1) the efficiency by which the power of sunlight is transferred to the antenna load (that is, to the diodes that provide rectification), and 2) the efficiency by which the captured light is transformed into DC power.

Antenna modelling

In this section, we focus on the first of these two points. First, we define a figure of merit (FOM) that allows us to objectively measure the performance of an antenna in the framework of energy harvesting and to optimize the design of such antennas. Then, we review some very general theoretical antenna concepts that

are useful to guide the design of harvesting antennas. Finally, we show an example of an antenna layout that, at least numerically, has a particularly promising performance.

The FOM we consider most appropriate for measuring an antenna's performance is the 'receiving efficiency,' which we define as follows. We consider a configuration consisting of a theoretically infinite two-dimensional array of antennas. Each antenna in the array is terminated with a load (i.e., the rectifying diode). The receiving efficiency is the ratio between the optical power transferred to the load of each antenna and the incident solar power on an area equal to that of the unit cell in the infinite array. In this way, the efficiency is uniquely defined, independently of the number of antennas in the array and the total area illuminated by sunlight.

Here, $S(\lambda)$ is the power spectral density of sunlight.[9]

$$\eta = \frac{\int_0^\infty \eta_{RX}(\lambda)S(\lambda)d\lambda}{\int_0^\infty S(\lambda)d\lambda} \quad \text{where} \quad \eta_{RX}(\lambda) = \frac{P_{LOAD}(\lambda)}{P_{INCIDENT}(\lambda)}$$

Equation 4

Readers will notice that this way of measuring antenna performance differs from methods used in several papers that have appeared in open literature, see for instance refs[8,10,11] In those papers, antennas were regarded as transmitting devices, and transmitting efficiency was used:

$$\eta_{TX}(\lambda) = \frac{P_{RAD}(\lambda)}{P_{ACCEPTED}(\lambda)}$$

Equation 5

In this definition, P_{RAD} is the amount of power that is radiated by an antenna and $P_{ACCEPTED}$ is the amount of power that enters the antenna terminals. We believe that the definition based on receiving efficiency is correct for two reasons. First, antennas for harvesting are essentially receiving devices. Second, and equally important, the transmitting efficiency completely neglects the antenna-to-load impedance matching.

The efficiency of reception can also be expressed differently to help understand how to design high-efficiency antennas. According to[12] :

$$\eta_{RX}(\lambda) = \frac{P_{LOAD}(\lambda)}{P_{INCIDENT}(\lambda)} = \frac{A_{eff}(\lambda)}{A_{eff}(\lambda)+A_{scatt}(\lambda)+A_{loss}(\lambda)}$$

Equation 6

Here, A_{eff}, A_{scatt} and A_{loss} are the effective, scattering, and loss areas of the receiving antenna, respectively. The effective area is the ratio between the power delivered to the load and the incident power. Similarly, the scattering area is the ratio between the scattered and the incident power. Finally, the loss area is the same for the portion of power lost due to Joule heating. Equation 6 shows that high efficiency can be achieved by minimizing losses and back-scattering from antennas. While reducing power lost to heating depends on the materials used to make the antennas and cannot be eliminated at optical frequencies due to significant losses in metallic materials, much can be done to minimize power lost to scattering. This observation is crucial for designing antennas for optical harvesting.

A general theorem of antennas[13] states that the effective area of an array of antennas can be at most half of the physical area occupied by the antennas. This means that the power transferred to the load of each antenna can be at most half

of the impinging power. Larger effective areas can be obtained if antennas are backed by a ground-plane and connected to matched loads.[14,15,16] In that case, the effective area of each antenna in an array can be as large as the area of the unit cell in the array occupied by the single antenna. In the absence of losses, this would account for an efficiency of up to 100% in Equation 6.

It should also be considered that, according to Equation 4, the overall efficiency of antennas for harvesting should be weighted by the spectral power density of solar radiation. This ranges roughly wavelengths from 3-400 nm to 2 μm, or equivalently, frequencies from 150 to 1000 THz, covering an extremely wide band. Here, a result obtained more than 50 years ago[14] regarding antenna arrays can further be used to guide antenna design.

In fact, it has been shown when antennas in an array are closely spaced and strongly interact with each other, the array can keep a stable performance even as the frequency or angle of incoming light changes.[15,16] Specifically, if the antennas are spaced less than 0.4 wavelengths apart, they can hold a steady resonant frequency no matter the direction of the incoming light. This setup causes the current across the entire plane of antennas to spread out in a consistent way. This uniform current flow makes the array act like a large, smooth-surfaced antenna, which is ideal for capturing a broad range of frequencies.[17]

The general characteristics of the antennas mentioned above suggest that, to achieve high-efficiency harvesting antennas, one must consider arrays of elements with inter-element spacing much smaller than the wavelength, placed above a reflector plane.

Figure 2 shows an example of an antenna design based on these guidelines. An array of optical antennas is arranged in a square lattice with pitch Λ. The antennas (violet shapes in the figure) are metallic square patches with a lateral dimension LA and thickness HA, placed on top of a dielectric substrate with thickness H_{DIEL} and relative dielectric constant ϵ_{DIEL}. A layer of metal beneath the dielectric substrate acts as a back-reflector. Red rectangles in the figure are loads, possibly diodes allowing for THz rectification. When choosing square aluminium antennas with a lateral size L_A = 72 nm and thickness H_A = 90 nm, a lattice with pitch Λ = 140 nm, and a substrate layer with relative permittivity ϵ_{DIEL}=2.25 and thickness H_{DIEL} = 71 nm, respectively, on top of a gold back-reflector, a theoretical receiving efficiency as high as 71% over the whole sun spectrum can be obtained.[18] This value is obtained by assuming that there are no detrimental effects due to loss of spatial coherence in sunlight, i.e. essentially that the total width of each array is smaller than the PCL.[19]
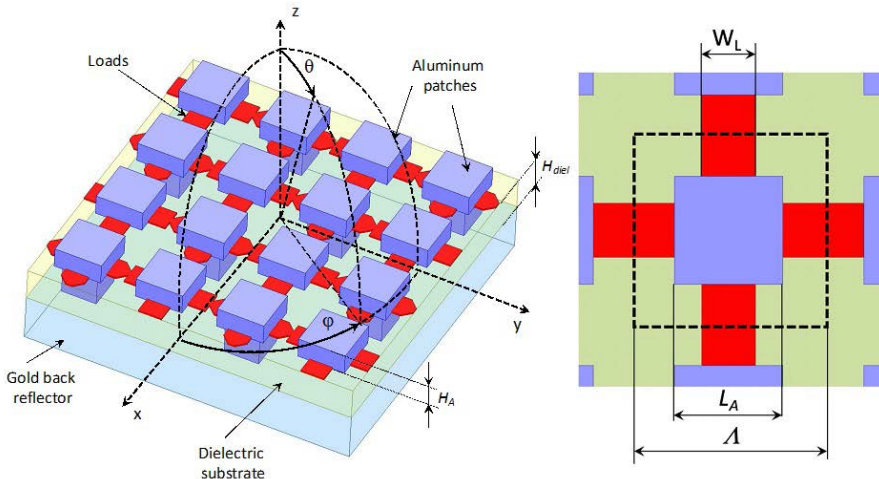

Figure 2.

Left: Schematic diagramme of an antenna array offering a theoretical reception efficiency of 71% over the entire solar spectrum.

Right: top view of the unit cell in the squared array. The detailed analysis of the antenna design and performance are reported in ref. [20]

This assumption is, of course, only partially valid. However, according to ref. 5, sunlight is spatially coherent over ~50 microns. With the array dimensions used in our design, this means that coherence is maintained over a set of about 20x20 antennas. This set is large enough to consider the infinite array approximation sufficiently accurate.

We highlight an essential aspect for achieving such high efficiency. The result was obtained assuming that the impedance of the diodes representing the load of the antennas was around 250 Ohm, which is optimal for matching with the internal impedance of the antenna array.

This impedance matching between the load and the antennas is of primary importance. To avoid the antennas back-scattering radiation from free space, causing loss of efficiency (see Equation 6), the antenna impedance needs to be in the same order as the free-space impedance, which is a few hundred ohms. Therefore, the diode load should also be in the same order to ensure reasonable matching. However, devices that can rectify radiation with frequencies in the tens or hundreds of THz, for example graphene ballistic or geometric diodes, often have impedances that are very different from the desired one. The sheet conductance of graphene at optical frequencies is in the order of the universal conductivity $\sigma_0 \approx 6 \cdot 10^{-5}$S,[21] yielding device impedance often in the tens of kOhm range.

Matching between antenna and load may possibly be improved by using well-known techniques, such as envisaging the employment of a dielectric layer that acts as an anti-reflection coating. However, many of the conventional matching techniques are narrowband. Also, quite often they cannot match loads with impedances differing by two or more orders of magnitude. This in turn, considering the high impedance (>1 kOhm) usually shown by geometric diodes, leads to the conclusion that matching between load and antenna impedance presently remains the most prominent and unresolved challenge for creating an efficient harvesting system.

Rectifier modelling

In this section we focus on the second part of the harvesting module i.e. rectification devices.

Geometric rectifiers[22] represent alternative class of rectifiers whose operation relies on the distinctive properties of ballistic transport. In high-mobility materials, charge carriers behave like "billiard balls"[23,24] and their trajectories can be influenced by the device's shape. By employing asymmetric geometric shapes (such as those depicted in Figures. 3(a) and 3 (c)), the back-scattering effects experienced by carriers differ when the current flow is reversed. This induces a device non-linear response, enabling rectification.

Due to their unique operating principles, geometric rectifiers are not subject to any threshold voltage (unlike classical pn junctions) and present a very small parasitic capacitance.[25] These characteristics make them capable of rectifying small and high-frequency signals, positioning them as promising candidates for energy harvesting applications.

According to the GreEnergy research and results, these devices have been investigated using different simulation strategy, namely:

→ pure coherent quantum-transport simulated by Scattering-Matrix/Landauer and DFT based approaches,
→ ballistic semi-classical approaches like Monte-Carlo
→ non-ballistic semi-classical approaches like drift-diffusion methods.

Drift-diffusion approaches are currently under test and will be object of further work, as they can help to investigate the "boundary" between quantum/ballistic behaviour and diffusive[26] behaviour. Monte-Carlo approaches are largely applied to demonstrate geometric rectification,[22] but they cannot account for interference effects, tunnelling effects, intra-band and inter-band coupling in a rigorous way. On the other hand, the case of pure quantum transport, although the related simulation is typically limited in terms of diode size (<100nm^2 area), is ideally expected as the most suitable and most effective for geometric rectification, as coherent travelling electron/hole waves are assumed to interact directly with the asymmetric discontinuities of the diode. Scattering of charges, namely multimode reflection and transmission, are the basis for current-voltage calculation.

Most of the modelling efforts have focused on two basic types of geometric rectifiers: the four-terminal rectifier (Figure 3a) and the two-terminal rectifier (Figure 3c). For the four-terminal rectifier, simulations were performed using a hybrid model combining Monte Carlo simulations with the Landauer-Büttiker formalism[27]. This approach was employed to identify the optimal geometric parameters configuration that maximizes the device response.[28] Specifically, Figure 3b illustrates an example, under ballistic transport conditions, of how the output voltage V_{LU} varies with the input voltage V_{SD} as geometric parameters are adjusted. Additionally, this model allowed for the simulation of the device response, incorporating the main scattering mechanisms typically present in CVD graphene deposited on an SiO$_2$ substrate.

A similar investigation was carried out for the two-terminal device, utilizing both quantum simulations based on the scattering matrix method[29] and self-consistent Monte Carlo simulations.[22] Figure 3d presents some I-V curves obtained from Monte Carlo simulations under ballistic conditions. The graph demonstrates that the non-linearity of the I-V characteristic increases with the angle a $_d$.
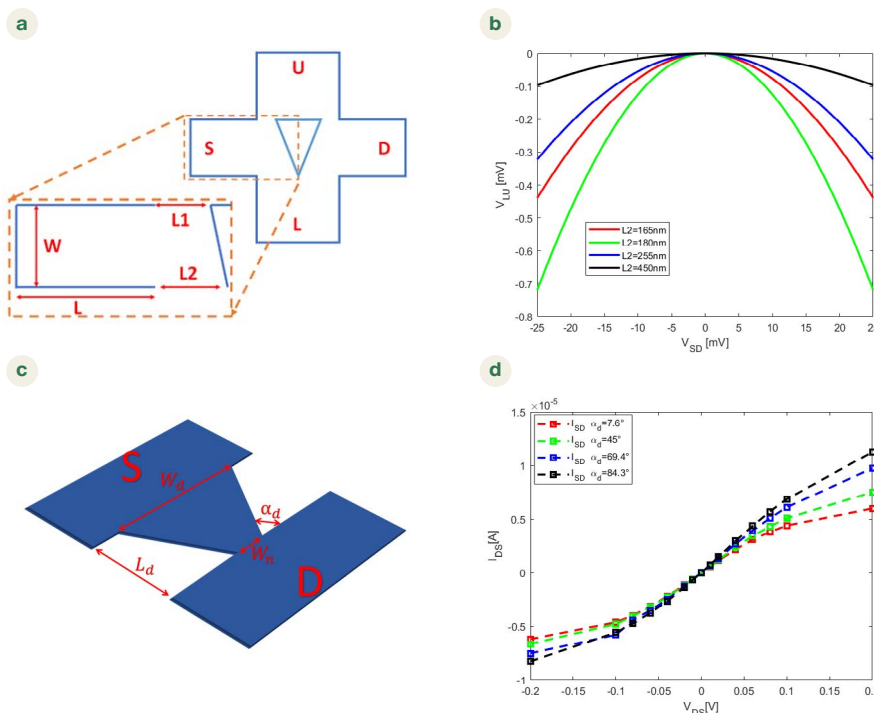
Figure 3. Four- and two-terminal rectifiers.

a) Sketch of the four-terminal rectifier. The input terminals are S and D while the output ones are U and L. W, L, L1 and L2 define the geometry of the structure;

b) Simulated trend of the output voltage (VLU) as a function of the input one (VSD) for ballistic transport regime and for different values of L2. The simulation considers W=100nm, L=100nm, L1=150nm and induced electron density n = 3x10^{11} cm^{-2};

c) Sketch of the two-terminal rectifier showing the main geometrical parameters;

d) Simulated I-V curve, in ballistic regime, for different values of the angle α_d, considering W$_d$=40nm, W$_n$=10nm.

Another interesting numerical example is the three-terminal rectifier (Figure 4a). This device has been simulated and evaluated in terms of I-V characteristics (Figure 4b), and specifically in terms of achievable short-circuit current and open circuit voltage[23]. Results of Figure 4 are obtained for a junction with W=10 nm. This kind of analysis allows to describe the behaviour of the junction when a generic load is applied, which corresponds to an output voltage different from zero, and potentially, to large impedance values, i.e. open circuit terminal. In Figure 4a we can see the output current as a function of the input and output voltage, corresponding to a finite output impedance.

It could be interesting to consider the intersection of the $I_{out}(V_{out})$ curve for a fixed input V_{ds}: an output load of a few kOhm (8 kOhm in the example of Figure 4d) sets the output voltage to a value which is about one order of magnitude smaller than the amplitude of the input voltage. The above considerations need to be extended to the case of high-frequency input voltage, by a rigorous quantum model, which is object of current and future work.
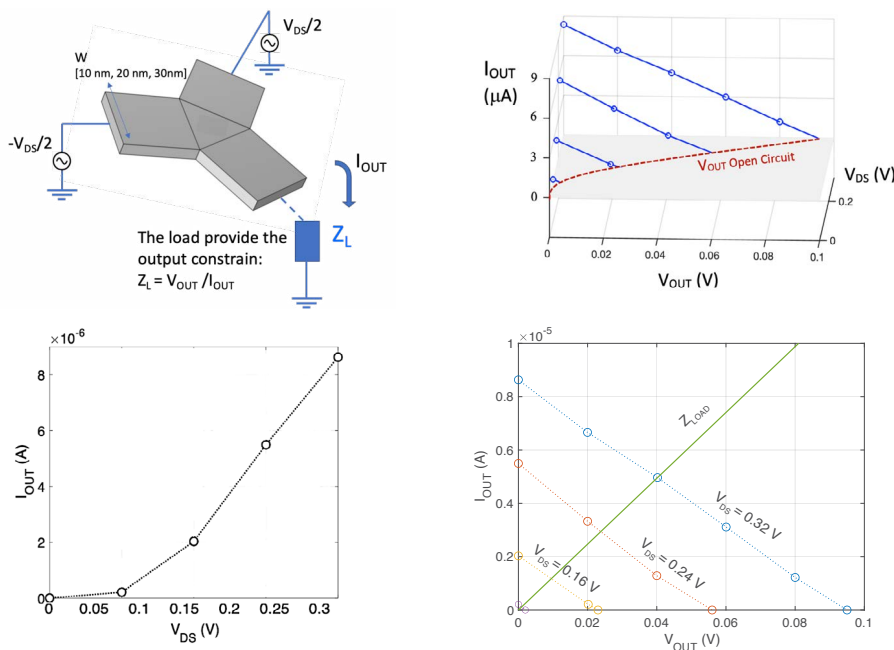

Figure 4.
Three-terminal rectifier.

a) Sketch;

b) output current as a function of input voltage (V_{DS}) and output voltage (V_{OUT});

c) short circuit current;

d) working point with an 8 kOhm load (d), for a Y junction with W=10 nm.

Rectenna prototyping

The working principle of ballistic rectifiers relies on a long charge carrier mean free path with respect to the overall device dimensions. This condition has so far been elusive in practical, scalable, devices because charge carriers in conventional materials typically have comparatively short mean free path lengths under ambient conditions. For instance, typical lateral device feature sizes achievable with common nanofabrication methods range between 2 μm (optical lithography) to 20 nm (electron beam lithography). At the same time, the typical mean free path length of electrons in Si at room temperature is between 10-30 nm.[30] Feasible fabrication of ballistic devices thus hinges on the availability of materials with a carrier mean free path length on the order of micrometres.

The discovery of graphene in 2004[31] and the subsequent successes in large-scale, high quality graphene growth by chemical vapor deposition introduced a new material platform capable of realizing ballistic transport over manufacturable device dimensions under ambient conditions. In CVD-grown graphene, mean free path lengths of over 28 μm have been demonstrated.[32]

Integrating graphene into electric devices faces several challenges. These include issues related to the transfer of graphene from the growth substrate to the target substrate, unwanted doping of the graphene channel, patterning the geometric diode neck, and forming ohmic contacts to graphene.

The resist mask used to pattern the small neck in geometric diodes and the triangular antidots in ballistic rectifiers requires a high-resolution electron beam lithography to reach critical dimensions in the order of nanometres.

Both at the input and output terminals of the rectifier, ohmic contacts need to be formed to the graphene channel. While metals deposited directly on top of graphene tend to form imperfect contacts mediated by van der Waals forces only, lateral contacts to the exposed graphene edge have been shown to reach a low contact resistance of 1.4 $\Omega\mu m^2$.[33] We have therefore perforated the graphene contact area with a pattern of holes to increase its effective edge length before metal deposition, thus forming a large number of edge contacts.

In GreEnergy, we employed commercial CVD-grown, large area graphene on a copper surface. We performed a wet transfer onto a high-resistivity Si/SiO_2 target substrate, ensuring that the substrate contributes only negligible absorption of the terahertz radiation during measurement.

By means of e-beam lithography we define the different graphene structures using negative electron beam lithography, including geometric diodes, ballistic rectifiers, along with test and control structures and devices to characterize the graphene quality and contact quality in-situ.

The exposed resist mask protects graphene from a subsequent oxygen plasma dry etching step and provides additional adhesion to the substrate during subsequent fabrication steps.

A second positive electron beam lithography defines the areas for metal deposition, i.e., contacts and antennas. Before the deposition, remaining resist from the graphene etching lithography step is removed from the exposed graphene with wet etching. The metal layer is deposited using electron beam evaporation, followed by a lift-off in a suitable organic solvent. A photograph of a finished wafer is shown in Figure 5. Using this fabrication process,[34] we reach mean free path lengths between 40-60 nm in devices using commercial CVD graphene. This is similar to the mean free path reported in other ballistic graphene rectifiers, which are usually based on exfoliated graphene. While the mean free path length in our rectifier and those in literature tend to be much shorter than the theoretical maximum, it does highlight the viability of our fabrication process.
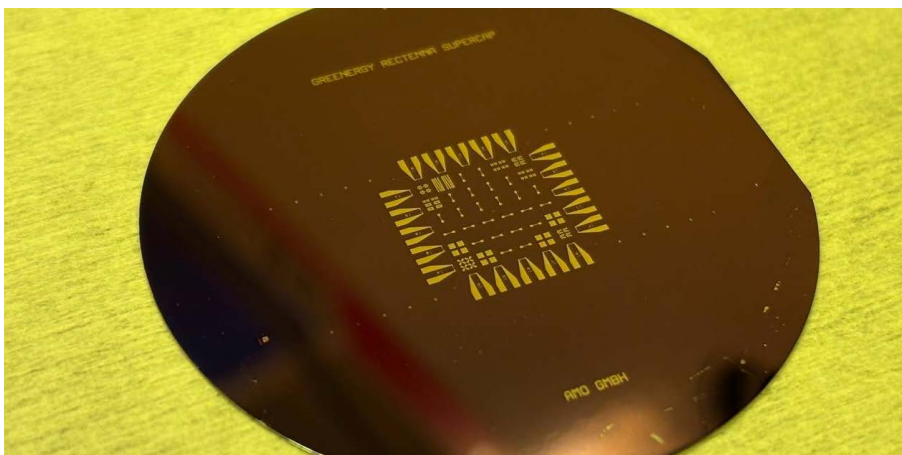

Figure 5. Photograph of a 2-inch wafer containing a number of THz rectennas.

The large pads around the edge of the square in the centre are contact pads to which the energy storage units are connected in subsequent fabrication steps.

Comments on graphene as diode material

With an eye to future commercial applications of solar rectenna technology, a number of fabrication challenges must certainly be addressed. These include the issue of assuring repeatably high graphene quality, large-scale graphene transfer, scalable nanolithography processes, and environmental encapsulation.

Commercially-grown CVD graphene still suffers from large batch-to-batch variations in key benchmarking quantities, such as Dirac point, defect density, double-layer density, wrinkles, and grain boundary size. This leads to a similarly large variation in mean free path length, one of the most important determining the efficiency of the rectenna device. The efficiency is further affected by the contact and sheet resistance of the graphene channel, thus complicating impedance matching techniques.

Large-scale rectenna arrays also require large-scale graphene areas with a high enough defect-free coverage to ensure sufficiently high device yield. This could be achieved either through large-scale graphene transfer techniques or direct growth on suitable substrates. Transfer processes that have been demonstrated on wafer-scale yet remain challenging and unreliable from a manufacturing perspective. Direct growth on insulating substrates is promising yet faces its own unique challenges: graphene growth is often fragile due to a large lattice mismatch between growth substrate and graphene.

All graphene geometric rectenna devices to date rely on electron beam lithography for the patterning of the rectifier structure. While electron beam lithography provides excellent lateral resolution in research settings, it is not competitive in terms of throughput and cost with scalable lithography methods, especially conventional stepper photolithography. Nanoimprint lithography is well-suited for large-scale, high-resolution patterning of graphene nanostructures,[35,36] in particular graphene geometric rectennas. The results achieved in the GreEnergy project demonstrate that acceptable ballistic rectification can occur also if the device is slightly larger than the mean free path length. While the rectification efficiency is reduced accordingly, the response at THz frequencies is nevertheless comparable to that previously achieved with exfoliated graphene.[37]

Rectenna devices in the real world need to reckon with ambient, even elevated temperatures, oxygen, and humidity. Adsorbed water in particular introduces additional chemical doping to the graphene layer, thus shifting the Dirac point further towards positive voltages. Exposure to oxygen can further damage existing graphene pinholes, grain boundaries, and cracks. These influences can in principle be protected against through appropriate encapsulation. In research settings, the 2D material hexagonal boron nitride (hBN) is often used as an encapsulation for graphene to improve its charge carrier mobility. In scalable fabrication, hBN growth and transfer unfortunately face similar challenges as in the case of graphene. Dielectric encapsulation methods could, however, feasibly protect the graphene layer from environmental influences while preserving graphene's high mobility. For example, alumina (Al_2O_3) or silica (SiO_2) are often used as dielectric encapsulation materials for graphene.[38, 39]

Energy storage prototyping and integration with rectenna

Integration of microsupercapacitors (MSCs) with on-chip energy harvesters can improve the lifetime of wireless sensor nodes in e.g. an Internet-of-Things (IoT) architecture. However, then MSCs should be fabricated through a complementary-metal-oxide-semiconductor (CMOS) compatible technology, ubiquitous in electrode choice with the capability of heterogeneous stacking of electrodes for modulation in properties driven by application requirements. Both these issues can be addressed through fabrication of multielectrode modular, high-energy density MSCs containing reduced graphene oxide (GO), and GO based electrodes, through a high wafer-yield spin coating process.[40]
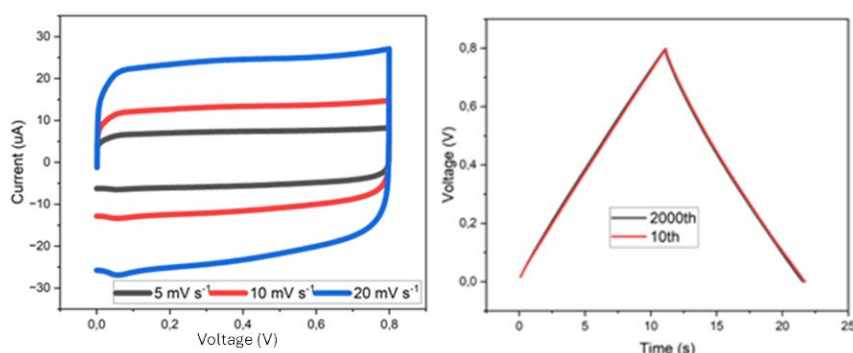

Figure 6. Measurements of IrO2 electrode devices

Left: the cyclic voltammetry at different voltage scan rates shows high quality semi-rectangular behaviour corresponding to a capacitance of about 7 mF•cm^{-2}.

Right: two charge-discharge curves at different points in the cycling show near identical features, demonstrating high device stability.

A problematic issue with the choice of carbon based electrodes is that it is difficult to reduce the required processing temperature down to below a few hundred degrees centigrade.[35] In the case where the MSC is expected to be integrated with devices that have restrictions on the thermal budget, this imposes processing challenges that risk inducing higher cost in production, and which could also result in both reduced performance and deterioration in reliability and lifetime for the integrated system. One very interesting electrode material in this respect is IrO_2, which has been employed as a high performing and robust material in challenging fabrication- and operation conditions.[41] We have within GreEnergy shown that MSC devices with IrO_2 electrodes provide competitive performance, with a specific capacitance of around 7 mF·cm^{-2} with negligible capacitance deterioration over 2000 cycles (Figure 6). We have also demonstrated that these MSCs can be integrated on the same chip as the harvesting units.

For some niche applications, like solar driven microdrones, it is important to achieve maximum power conversion at minimum weight. Here light-weight carbon fibres could provide the thin film substrate that would carry the solar harvesting device layers, while also providing function as wings and energy storage. We have shown how such carbon fibres can simply be produced from an appropriate mix of cellulose and lignin precursor.[42]

When addressing the challenge of fabricating an integrated system where solar harvesters and energy storage components are combined in one device, it is important to look at relevant application scenarios for arriving at how to prioritize trade-offs and which performance parameters to give precedence. (In many cases there is simply no need, nor any benefit, of integrating the storage component on the harvester chip).

There are several recent examples of integrated systems with photovoltaic sunlight harvesting combined with MSC storage. Weiwen Wang et al. reported the fabrication of a self-powered integrated system consisting of an MSC, solar cell and a heartbeat sensor[43]. The supercapacitor was fabricated using $Ti_3C_2T_x$/CNTs and exhibited large capacitance ~605 mF cm^{-2} in the potential window of 0.8 V. Two such supercapacitors were connected in series and then charged to 1.6 V using a commercial solar cell. The supercapacitors were discharged in 88 s under 3 mA cm^{-2} constant current density, which was sufficient for sensor operation. Pengcheng Sun et al. demonstrated the fabrication of N doped NiS and MXene based asymmetric supercapacitor via inkjet printing.[44] The fabricated device performed well in 1.5 V potential window and tested for solar charging ability. The supercapacitor was connected to a commercial solar cell and charged to 1.2 V under sunlight as well as lamp light. It was found that supercapacitor showed better efficiency, when charged by sunlight. Chung Lee et al. demonstrated the fabrication of an all-in-one device by combining a silicon solar cell and a supercapacitor with polymer gel electrolyte[45] . The supercapacitor was solar charged for 100 s and then investigated for self-discharge profile.

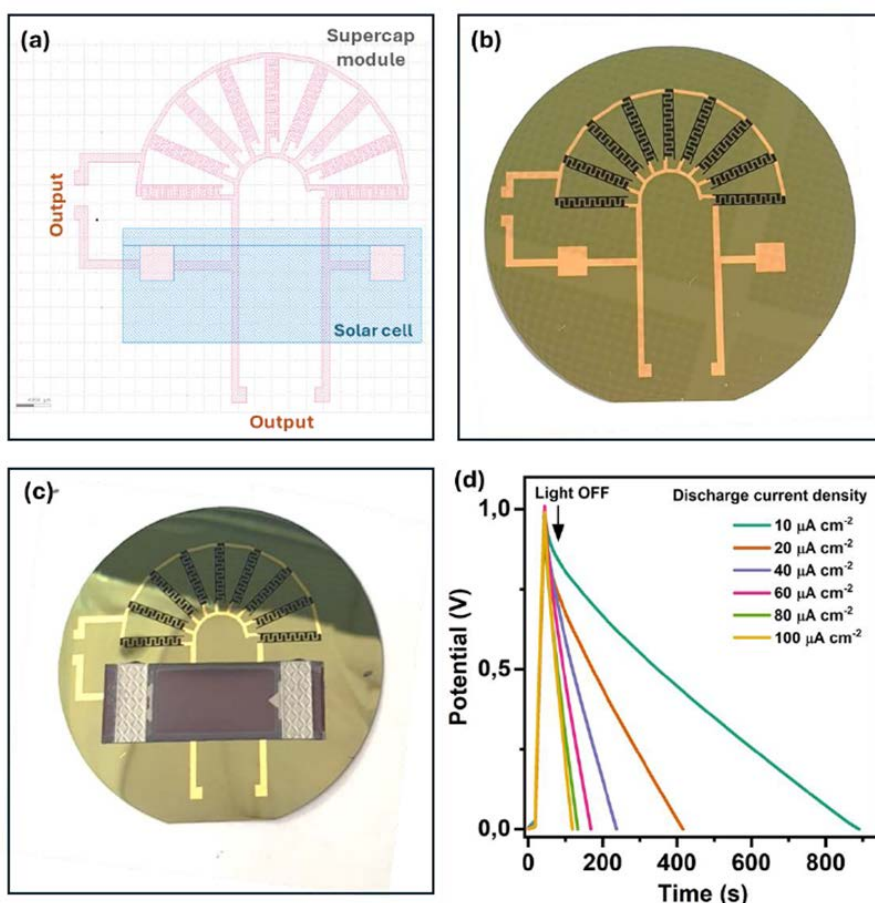

Figure 7. A prototype demonstrator having solar cell and SC module integrated on the same chip.

a) Schematic design layout;

b) image of the fabricated 2-inch wafer with SC module on it;

c) image of the SC module and solar cell mounted on the same chip ;

d) chronopotentiometry measurements performed under light ON/OFF conditions.

We have shown that our IrO_2 based MSCs can be combined with commercial photovoltaic cells (INP1.2-12X34, PowerFilm Inc.). Figure 7 shows a set of parallelly connected capacitors manufactured by lithography on a silicon wafer, connected with the photovoltaic cell together with sample charge-discharge characteristics. A PVA-H_3PO_4 gel electrolyte was drop-casted on the electrodes and the charging experiments were performed multiple times (3-5 times) on the same device over a period of one week to ensure the reproducibility and stability of the devices.

Circuitry

To transfer the harvested power to the output of the system with minimum loss, all the fabricated elements should work to provide optimum power transfer. In that sense, the power management unit (PMU) is a crucial component in the system. The development of a practical harvester is only possible if a proper circuitry is used as PMU, which can be a passive matching circuitry or a self-powered voltage regulator. While an active circuitry uses some of the collected power to functionalize the system further, a passive circuitry can be used as matching block between the elements without using any of the collected power. With this perspective, the passive matching seems to be the way to proceed to pursue maximum efficiency.

The main challenge for the circuit design is to create proper electrical models of the fabricated devices (antennas, diodes and storage elements). These models can then be used to design a circuit for the maximum power transfer characteristics, as well as impedance matching. Moreover, using these models, several possible matching circuitries as well as rectenna array structures can be simulated and proposed for the system level design.

In the light of the requirements we have created electrical models from the fabricated devices (antenna, diode, rectenna and supercapacitor) and used these devices to propose maximum power transfer passive matching circuits and rectenna arrays. Up to now, it has been shown that the modelling of the fabricated devices is matching with the measurement results, and they can be easily inserted in the testbench for further simulations. The developed simulation testbench is versatile and adaptable, and a powerful tool for a wide range of applications simulations.

Conclusions and outlook

In the GreEnergy project we have taken several important steps towards a future solar-antenna based energy harvesting system. Our design and simulations of novel antenna structures, geometries, and, importantly nanoantenna arrays with back-reflectors, should in principle provide high enough absorption of solar radiation. The fabrication of required nanometre structures needs further development, both regarding resolution and, in a longer perspective, upscaling. Electron beam lithography must eventually be replaced by some high throughput nanolithography technology, if nano-antenna arrays are ever to be cost-effective.

When it comes to the ultrahigh speed rectifiers, the challenges are even greater. We have chosen to explore, the still immature concept, of geometrical diodes based on ballistic transport in single layer graphene. In theory, single crystal graphene, i.e. graphene without any defects, should provide high enough charge-mobility for such diodes. But inevitably, as the layer is one atom thick, all its atoms are under influence from the surrounding that acts like "doping" of the graphene. Hence, the properties of graphene are in general heavily, and detrimentally, influenced by the neighbouring materials. This makes it very difficult to reach the required mean free path lengths of charges for ballistic transport in real devices. This problem could be partly solved by shrinking the size of the diodes further, which of course on the other hand makes the fabrication of the diodes even more challenging.

As mentioned above, dedicated encapsulation of the graphene layer by means of e.g. single layer hexa-boron nitride has been shown to provide significantly enhanced charge mobility. However, at present we see no possibility of upscaling of this encapsulation method.

With future upscaling in mind, we have focussed on CVD-grown graphene. But even if the quality of the graphene on the growth substrate can further improved in the future, the transfer and further processing of the graphene layer introduces defects which reduce charge mobility. In this view, it would be preferred to be able to grow, or synthesize, graphene directly on the device chip itself, which should be a topic of future work.

A remaining task, of utmost importance, is the necessary impedance matching between the nano-antenna arrays and the diodes to minimize the losses. But before this problem can be fully tackled, the characteristics of the individual components, especially the ballistic diodes, must be improved in terms of inherent losses. Reduction of the contact resistances, e.g. between metals and graphene, stand out as one of the key issues.

Once rectennas with sufficient performance are realized, our work suggests that these could, if necessary be integrated with further electronics, e.g. storage units such as supercapacitors. However, we are of course aware of the fact that the trade-off between effective use of device area and overall efficiency must be considered.

References

1. Davenport, J. & Wayth, N. *2024 Statistical Review of World Energy*. (Energy Institute, 2024).

2. World Energy Resources: Solar World Energy Council 2013.

3. Bailey, R. L. A proposed new concept for a solar-energy converter. *J. Eng. Gas Turbines Power* **94**, 73–77 (1972).

4. Proposal number 101006963.

5. S. Divitt et al., Spatial coherence of sunlight and its implications for light management and photovoltaics, Optica, **2**, 95-105 (2015).

6. A. A. Vyas et al., On-Chip Interconnect Conductor Materials for End-of-Roadmap Technology Nodes, IEEE Trans. On Nanotechnology, **17**, 4-10 (2018).

7. D. Gall, et al., Materials for interconnects *MRS Bulletin* **46**, 959-966 (2021).

8. Z. K. Ma and G. A. Vandenbosch, "Optimal solar energy harvesting efficiency of nano-rectenna systems," *Sol. Energy* **88**, 163–174 (2013).

9. C. Gueymard, D. Myers, and K. Emery, "Proposed reference irradiance spectra for solar energy systems testing," *Sol. Energy* **73** (6), 443–467 (2002).

10. G. A. Vandenbosch and Z. Ma. Upper bounds for the solar energy harvesting efficiency of nano-antennas. *Nano Energy*, **1** (3):494– 502, (2012).

11. H. Zhao, H. Gao, T. Cao, and B. Li. Efficient full-spectrum utilization, reception and conversion of solar energy by broad- band nanospiral antenna. *Opt. Express*, **26** (2):A178–A191, (2018).

12. A. Balanis, *Antenna Theory, 3rd edition*, John Wiley and Sons, 2005, section 2.15.2.

13. S. A. Schelkunoff and H. T. Friis, *Antenna Theory and Practice* (John Wiley and Sons, 1952).

14. B. A. Munk. Periodic surface for large scan angles. US Patent 3789404A, 1968.

15. B. A. Munk. Frequency Selective Surfaces, Theory and Design. John Wiley and Sons, 2000.

16. B. A. Munk. Finite Antenna Arrays and FSS. John Wiley and Sons, 2003.

17. H. A. Wheeler, "Simple relations derived from a phased array antenna made of an infinite current sheet," *IEEE Trans. Antennas Propag.* **13**, 506–514 (1965).

18. M. Midrio, L. Pierantoni, S. Boscolo, D. Truccolo and D. Mencarelli, "Nano-antenna array for high efficiency sunlight harvesting", *Opt. Expr.*, **30** (5):7017-7034, (2022).

19. B. A. Munk. Finite Antenna Arrays and FSS. John Wiley and Sons, 2003.

20. M. Midrio, L. Pierantoni, S. Boscolo, D. Truccolo and D. Mencarelli, "Nano-antenna array for high efficiency sunlight harvesting", Opt. Expr., 30(5):7017-7034, (2022).

21. G. Hanson, "Dyadic Green's functions and guided surface waves for a surface conductivity model of graphene", *J. Appl. Phys*, **103**, 064302 (2008).

22. A.M.Song, A.Lorke, A. Kriele, J.P.Kotthaus, W.Wegsheider., M. Bichler, Non-linear electron transport in an asymmetric microjunction: a ballistic rectifier *Phys. Rev. Lett.*, **80** 3831-3834 (1998).

23. Beenakker, C. W. J., and Henk van Houten. "Quantum transport in semiconductor nanostructures." *Solid state physics*. **44**. Academic Press,. 1-228 (1991).

24. Song, Aimin M. "Room-temperature ballistic nanodevices." *Encyclopedia of Nanoscience and Nanotechnology*. **9**. No. 389. American Scientific Publishers, 2004. 371-389.

25. Zhu, Zixu, et al. "Graphene geometric diodes for terahertz rectennas." *Journal of Physics D: Applied Physics* **46**.18 (2013): 185101.

26. D. Truccolo et al, IEEE TRANSACTIONS ON ELECTRON DEVICES, **71**, NO. 2, FEBRUARY 2024.

27. Büttiker, M. «Four-terminal phase-coherent conductance." *Physical review letters* **57**.14 (1986): 1761.

28 Truccolo, D et al., *Solid-State Electronics* **194** (2022): 108314.

29 D. Mencarelli et al, IEEE Access, **10**, pages 123251-7, 2022.

30 Custer, James P., Jeremy D. Low, David J. Hill, Taylor S. Teitsworth, Joseph D. Christesen, Collin J. McKinney, James R. McBride, Martin A. Brooke, Scott C. Warren, and James F. Cahoon. "Ratcheting Quasi-Ballistic Electrons in Silicon Geometric Diodes at Room Temperature." *Science* **368**, no. 6487 (April 10, 2020): 177–80.

31 Novoselov, K. S. et al. Electric Field Effect in Atomically Thin Carbon Films. *Science* **306**, 666–669 (2004).

32 Banszerus, L., M. Schmitz, S. Engels, M. Goldsche, K. Watanabe, T. Taniguchi, B. Beschoten, and C. Stampfer. "Ballistic Transport Exceeding 28 Mm in CVD Graphene. *Nano Letters* **16**, no. 2 (2016): 1387–91.

33 S. Behera, Pure edge-contact devices on single-layher-CVD-graphene integrated into a single chip. *Scientific Reports*, **13**, 10588 (2023).

34 Passi, V., Gahoi, A. & Lemme, M. C. Enhanced asymmetry in monolayer graphene geometric diodes. in *2017 Silicon Nanoelectronics Workshop (SNW)* 137–138 (2017).

35 X. Liang et al. Formation of bandgap and sub-bands in graphene nanomseshes with sub-10nm ribbon width fabricated via nanoimprint lithography, *Nano Lett.* **10**, 2454-2460 (2010).

36 D.M. Mackenzie et al., Batch fabrication of nanopatterned graphene devices via nanoimprinit lithography, *Appl. Phys. Lett.*, **111**, 193103 (2017).

37 Auton, G. et al. Terahertz Detection and Imaging Using Graphene Ballistic Rectifiers. *Nano Lett.* **17**, 7015–7020 (2017).

38 K. Dockx et al. Strong doping reduction on waver-scale CVD graphene devices via Al2O3 ALD encapsulation. *Nanotechnology*, **35**, 395202 (2024).

39 S. B. Kalkan et al., Impact of encapsulation method on the adsorbate induced electrical instability of monolayer graphene. *J. Vac. Sci. Technol.* A **37**, 051502 (2019).

40 A. Vyas et al., Spin-Coated Heterogenous Stacked Electrodes for Performance Enhancement in CMOS-Compatible On-Chip Microsupercapacitors *ACS Applied Energy Materials* **2022** 5 (4), 4221-4231.

41 Jimin Maeng et al 2019 *Meet. Abstr.* MA2019-01 89.

42 A. Rajaras et al., "The Influence of Hardwood Lignin Blending on the Electrical and Mechanical Properties of Cellulose Based Carbon Fibers", *ACS Sustainable Chem. Eng.*, **12**, Issue 30, 11206–11217, (2024).

43 W. Wang, L. Xu, L. Zhang, A. Zhang, J. Zhang, Self-Powered Integrated Sensing System with In-Plane Micro-Supercapacitors for Wearable Electronics, *Small* **19** (2023) 2207723.

44 P. Sun, J. Liu, Q. Liu, J. Yu, R. Chen, J. Zhu, G. Sun, Y. Li, P. Liu, J. Wang, An inkjet-printing ink based on porous NiS/N-MXene for high-performance asymmetric micro-supercapacitors and self-powered microelectronics, *Chem. Eng. J.* **474** (2023) 145466.

45 C. Lee, I. Subiyanto, S. Byun, S.O. Han, C.-H. Cho, H. Kim, Enhanced Energy Density in All-in-One Device Integrating Si Solar Cell and Supercapacitor Using [BMlm] CI/PVA Gel Electrolyte, *ACS Omega* **9** (2024) 7255–7261.

Project publications

1. Truccolo, D., Palestri, P., Esseni, D., Boscolo, S. & Midrio, M. Comprehensive Analysis of Graphene Geometric Diodes: Role of Geometrical Asymmetry and Electrostatic Effects. IEEE Trans. Electron Devices **71**, 1294–1301 (2024).

2. Mohebbi, E. et al. Towards graphene-based asymmetric diodes: a density functional tight-binding study. Nanoscale Adv. **6**, 1548–1555 (2024).

3. Azega, R. K. A. et al. Influence of Hardwood Lignin Blending on the Electrical and Mechanical Properties of Cellulose Based Carbon Fibers. ACS Sustain. Chem. Eng. **12**, 11206–11217 (2024).

4. Azega, R. K. et al. Supercapacitors and rechargeable batteries, a tale of two technologies: Past, present and beyond. Sustain. Mater. Technol. **41**, e01111 (2024).

5. Zampa, G. M., Mencarelli, D. & Pierantoni, L. A full-wave time-dependent Schrödinger equation approach for the modeling of asymmetric transport in geometric diodes. Phys. B Condens. Matter **661**, 414917 (2023).

6. Pérez Caballero, L. M. et al. Developing the next generation of renewable energy technologies: an overview of low-TRL EU-funded research projects. Open Res. Eur. **3**, 8 (2023).

7. Pecunia, V. et al. Roadmap on Energy Harvesting Materials. J. Phys. Mater. **6**, 042501 (2023).

8. Azega, R. K. et al. Effect of plasma treatment on electrochemical performance of lignin-based carbon fibers. J. Electroanal. Chem. **946**, 117723 (2023).

9. Vyas, A. et al. Spin-Coated Heterogenous Stacked Electrodes for Performance Enhancement in CMOS-Compatible On-Chip Microsupercapacitors. ACS Appl. Energy Mater. acsaem.1c03745 (2022).

10. Vyas, A. On-chip electrochemical capacitors and piezoelectric energy harvesters for self-powering sensor nodes. (Chalmers University of Technology, Department of Microtechnology and Nanoscience, Göteborg, Sweden, 2022).

11. Saeed, M. et al. Graphene-Based Microwave Circuits: A Review. Adv. Mater. 2108473 (2022).

12. Rozzi, T., Mencarelli, D., Zampa, G. M. & Pierantoni, L. Dirac-Based Quantum Admittance of 2D Nanomaterials at Radio Frequencies. Appl. Sci. **12**, 12539 (2022).

13. Midrio, M., Pierantoni, L., Boscolo, S., Truccolo, D. & Mencarelli, D. Nano-antenna array for high efficiency sunlight harvesting. Opt. Express **30**, 7017 (2022).

14. Mencarelli, D., Zampa, G. M. & Pierantoni, L. Current-Voltage Characterization of Multi-Port Graphene Based Geometric Diodes for High-Frequency Electromagnetic Harvesting. IEEE Access **10**, 123251–123258 (2022).

15. Lemme, M. C., Akinwande, D., Huyghebaert, C. & Stampfer, C. 2D materials for future heterogeneous electronics. Nat. Commun. **13**, 1392 (2022).

16. Haque, M. et al. Exploiting low-grade waste heat to produce electricity through supercapacitor containing carbon electrodes and ionic liquid electrolytes. Electrochimica Acta **403**, 139640 (2022).

17. Vyas, A. et al. Alkyl-Amino Functionalized Reduced-Graphene-Oxide–heptadecan-9-amine-Based Spin-Coated Microsupercapacitors for On-Chip Low Power Electronics. Phys. Status Solidi B 2100304 (2021).

18. Pierantoni, L. et al. Dirac Equation-Based Formulation for the Quantum Conductivity in 2D-Nanomaterials. Appl. Sci. **11**, 2398 (2021).

19. Hemmetter, A. et al. Terahertz Rectennas on Flexible Substrates Based on One-Dimensional Metal–Insulator–Graphene Diodes. ACS Appl. Electron. Mater. acsaelm.1c00134 (2021).

GreEnergy

Power from optical antennas

www.greenergy.eu
info@greenery.eu